Microchimica Acta (2020) 187: 78
https://doi.org/10.1007/s00604-019-3997-1

ORIGINAL PAPER

A nanocomposite consisting of etched multiwalled carbon nanotubes, amino-modified metal-organic framework UiO-66 and polyaniline for preconcentration of polycyclic aromatic hydrocarbons prior to their determination by HPLC

Jianxiong Chen[1] · Birong Zhang[1] · Xueping Dang[1,2] · Dongyun Zheng[2] · Youhong Ai[1] · Huaixia Chen[1]

Received: 26 June 2019 / Accepted: 3 November 2019 / Published online: 2 January 2020
© Springer-Verlag GmbH Austria, part of Springer Nature 2020

Abstract

A polyaniline composite doped with etched multi-walled carbon nanotubes and UiO-66-NH_2 was prepared by electropolymerization. It was used as a sorbent to extract the polycyclic aromatic hydrocarbons (PAHs) phenanthrene, fluoranthene and pyrene. Its surface morphology, crystal structure and capability of adsorbing PAHs were characterized by scanning electron microscopy, X-ray photoelectron spectrometry, Fourier transform infrared spectrometry and zeta potentiometry. The π stacking and anion-π interactions are shown to play dominant roles in the sorption mechanism. Coupled with high performance liquid chromatography, the composite-modified fiber was applied to detect PAHs in lake water samples by direct immersion extraction. The method excels by (a) wide linear range (0.05–20 ng mL^{-1}), (b) low limits of detection (10 pg mL^{-1}), (c) satisfactory recovery from spiked samples (84.7–113.8%), and (d) good reproducibility (relative standard deviations of <6.5%). The method is superior in terms of costs and reproducibility compared to some pretreatment methods with mass spectrometric detection.

Keywords Polyaniline · UiO-66-NH_2 · Multiwalled carbon nanotubes · Solid phase microextraction · Chromatography

Introduction

Metal organic frameworks (MOFs) are crystal materials consisting of inorganic metal ions and organic ligand. Their morphology or pore-size distribution can be tuned by acid, surfactant or other ways [1–4]. Because of their tunable porosity and tailorable topology, MOFs have drawn broad attention in many fields [5–8]. However, some tuned MOFs have not good properties which restricted their applied range. For example, the crystalline structure of some MOFs was easy to break down after removal of the surfactant template [9]. Some mesoporous MOFs obtained by ligand extension were likely to collapse in the absence of guest molecules [10]. In addition, it was difficult to etch some unstable MOFs with acid to adjust their pore structure [11]. Therefore, it remains a great challenge to develop an effective strategy to enhance the properties of the tuned MOFs.

Multiwalled carbon nanotubes (MWCNTs) are tubular carbon materials with abundant π-systems, unique electrical properties and high specific surface properties [12]. It has been widely used in solid phase microextraction (SPME) [13], modified electrodes [14] and supercapacitors [15]. The doping of MWCNTs has been shown to improve the mechanical strength, thermal stability and chemical properties of the composites [16, 17]. Qasem, et al. synthesized MWCNT/MIL-101(Cr) composites for CO_2 capture and separation. The experimental results showed that the optimal ratio of MWCNT/MIL-101 to CO_2 adsorption capacity was 35% higher than that of pure MIL-101 [18]. Common methods for preparing

Electronic supplementary material The online version of this article (https://doi.org/10.1007/s00604-019-3997-1) contains supplementary material, which is available to authorized users.

✉ Xueping Dang
dangxueping@hubu.edu.cn

✉ Huaixia Chen
hxch@hubu.edu.cn

[1] Hubei Collaborative Innovation Center for Advanced Organic Chemical Materials, Ministry of Education Key Laboratory for the Synthesis and Application of Organic Functional Molecules&College of Chemistry and Chemical Engineering, Hubei University, Wuhan 430062, People's Republic of China

[2] Hubei Key Laboratory of Medical Information Analysis and Tumor Diagnosis & Treatment, Wuhan 430062, People's Republic of China

MWCNT composites include in-situ growth and physical blending, etc. It is still important to develop new approaches to broaden the applicability of carbon nanotubes.

Polyaniline (PANI) is another widely studied conductive polymer due to its adjustable properties and low raw materials [19, 20]. PANI has a multifunctional and permeable porous structure, which can provide different intermolecular interactions such as acid-base interactions, induction, hydrophobic interactions and hydrogen bonding. PANI can be directly electrodeposited on the metal surface. It can be easily modified by controlling electrochemical conditions, types of aniline monomers and dopant ions [21, 22]. Lu, et al. reported a new approach for the electropolymerization of aniline with the utilization of a MOF thin film [23]. The prepared porous PANI exhibited higher specific surface area than the pure MOFs. The approach provided a new route to prepare the composite of PANI and MOFs.

Polycyclic aromatic hydrocarbons (PAHs) are composed of two or more fused aromatic benzene rings. They are derived from oil spills, combustion of fossil fuel, timber and tobacco, as well as some chemical processes, *etc* [24, 25]. Based on the toxicity and potential hazard for human exposure, 16 types of PAHs have been classified as priority pollutants by United States Environmental Protection Agency (US EPA). Many researchers believed that some PAHs would be carcinogenic to humans [26, 27]. Zelinkova, et al. summarized the pathways of PAHs to contaminate food, including PAHs from air, soil and water, or food cooking and processing [28]. Freshwater is essential to maintain human health, so it is necessary to establish a highly sensitive and simple method for detecting PAHs in water source.

In this work, we describe a novel polyaniline composite doped with etched MWCNT/UiO-66-NH_2 on the surface of stainless-steel wire by electropolymerization. The PANI-etched MWCNT/UiO-66-NH_2 coated fiber was characterized by fourier transform infrared spectrometry (FT-IR), X-ray diffractometry (XRD) and scanning electron microscopy (SEM). The adsorption mechanism of PAHs on this composite was also investigated by infrared spectrometry, X-ray photoelectron spectrometer (XPS) and zeta potentiometry. The fiber was successfully applied for the detection of PAHs in lake water samples by direct immersion SPME (DI-SPME).

Experimental section

Reagents and supplies

Methanol and acetonitrile (HPLC/spectrograde) were purchased from the TEDIA (America, http://www.tedia.com.cn/). Ultra-pure water was produced from the ultra-pure water system (Beijing Epoch Electronic Instrument Co., Ltd., http://www.leeyuan.net/). Zirconium (IV) chloride ($ZrCl_4$, 98.0%), 2-aminoterephthalic acid (ATP, 98.0%), acetic acid glacial (HAc, 99.5%) and sodium dodecylbenzene sulfonate (SDBS, 92.5–100.5%) were purchased from Macklin Biochemical Co., Ltd. (Shanghai, China, http://www.macklin.cn/). MWCNTs (diameter: 20–40 nm, length: > 5 μm) were obtained from Shenzhen Nanotech Port Co., Ltd. (Shenzhen, China, http://www.nanotubes.com.cn/Cn/index.aspx). N, N-dimethylformamidel (DMF, 99.5%), ethanol (99.7%), aniline (ANI, 99.5%), sulfuric acid (H_2SO_4, 95.0–98.0%) and nitric acid (HNO_3, 65.0–68.0%) supplied from Sinopharm Chemical Reagent Co., Ltd. (Shanghai, China, http://www.sinopharm.com/), and ANI was purified through vacuum distillation before used. Phenanthrene (99.5%), fluoranthene (98.0%) and pyrene (99.0%) were purchased from Aladdin Co., Ltd. (Shanghai, China, https://www.aladdin-e.com/zh_cn/). All mobile phase and samples were filtered by polyvinylidene fluoride filter membrane (pore size: 0.22 μm, diameter: 50 mm. Jinteng Experimental Equipment Co., Ltd. Tianjin, China, http://tjtengda.biogo.net/).

Instruments

A CHI 830 electrochemical workstation (Shanghai Chenhua Instruments Co., Ltd., http://www.chinstr.com/sy) was employed for preparing coating. A conventional three-electrode system was used, including a stainless-steel wire (SS, 2.2 cm × 250 μm O.D.) as working electrode, a Pt electrode as counter electrode and a saturated calomel electrode (SCE) as reference electrode. A Dionex Ultimate 3000 high performance liquid chromatography system (HPLC) equipped with a six-way valve manual injector, a photodiode array detector (PAD), a column with a stationary phase of C18 (Welch Ultimate XB-C18, Dionex, US) and a column oven (LGC-1025 M, Dingtai Biochemical Technology Equipment Manufacturing Co., Ltd. Wuhan, China, http://www.dthschina.com/) was used for chromatographic analysis. Fourier transform infrared spectra were acquired using NICOLET iS10 spectrophotometer (Thermo Fisher Scientific, America, https://www.thermofisher.com/). Scanning electron microscopy experiments were carried out on a JSM7100F field-emission scanning electron microscope (JEOL, Japan, https://www.jeol.com.cn/) with an accelerating voltage of 15 kV. The surface charge of the composite changed with pH was measured by a Zeta potentiometer (ZS 90, Malvern Panalytical Ltd., England, https://www.malvernpanalytical.com.cn/). The pH of the solution was measured and adjusted by a pH meter (FiveEasy Plus, Mettler-Toledo International Ltd., https://www.mt.com/). The crystal structure of the composite was characterized by X-ray diffractometry (D8A25, Bruker, Germany, https://www.bruker.com/cn/). The change of the inner electron binding energy of the atoms before and after the composite adsorbed the target analytes was measured by X-ray photoelectron spectrometer (Escalab 250 Xi, Thermo Fisher Scientific, America, https://www.thermofisher.com/).

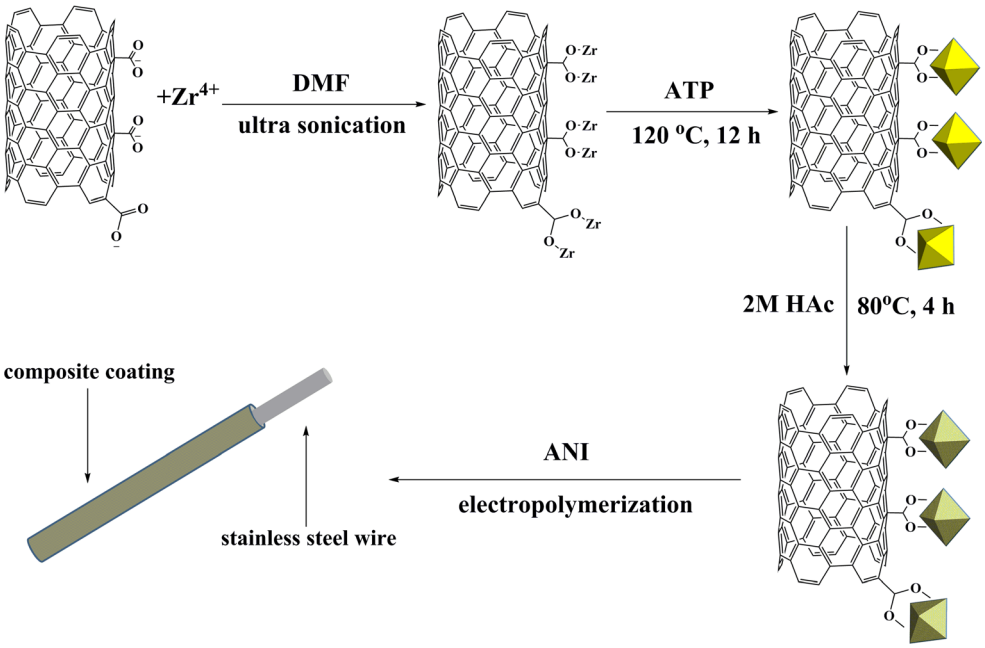

Fig. 1 The preparation process of PANI-etched MWCNT/UiO-66-NH_2 composite

Preparation of standard solution and water sample

The standard stock solutions of phenanthrene, pyrene and fluoranthene were prepared in methanol with the concentration of 1 mg mL^{-1}, which were stored at 4 °C. The daily standard working solutions were obtained by diluting standard stock solution with ultra-pure water for use.

The water samples were collected from ShaHu Lake and Yanxi Lake in Wuhan (Hubei, China). All samples were filtered and stored at 4 °C.

Preparation of SPME fiber

Preparation of etched MWCNT/UiO-66-NH_2 composites

20 mg carboxylated MWCNTs (the carboxylation procedure was in supplementary materials) were added to 80 mL DMF solution containing 660 mg $ZrCl_4$. After ultrasonic dispersion for 20 min, 520 mg ATP was added and the ultrasonic dispersion was continued for 20 min. The solution was put into a Teflon-lined reactor, which was placed in the oven at 120 °C for 24 h to obtain MWCNT/UiO-66-NH_2 composite. The obtained composite was washed for 10 times with ethanol, then it was placed in a vacuum oven for drying at 70 °C overnight.

100 mg dried MWCNT/UiO-66-NH_2 was put into a Teflon liner containing 10 mL of 2 M HAc solution for being etched for 4 h in an oven at 80 °C. The etched composite was washed for 10 times with ethanol and dried under vacuum at 70 °C overnight.

Preparation of PANI-etched MWCNT/UiO-66-NH_2 composite

A stainless-steel wire as working electrode was washed in 0.5 M H_2SO_4, 1 M NaOH and ultrapure water for 20 min successively. The electrolyte solution comprised 10 mL of 0.5 M HNO_3, 10 mg etched MWCNT/UiO-66-NH_2, 50 mg SDBS and 90 μL of ANI. The three-electrode system was placed in the electrolyte solution. Then the electropolymerization was performed by cyclic voltammetry at scan rate of 100 mV s^{-1} for 80 circles with the potential range of −0.2-1.2 V. After the

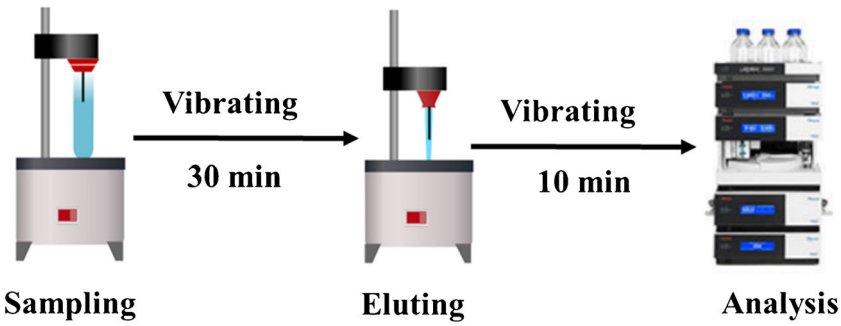

Fig. 2 SPME-HPLC procedure

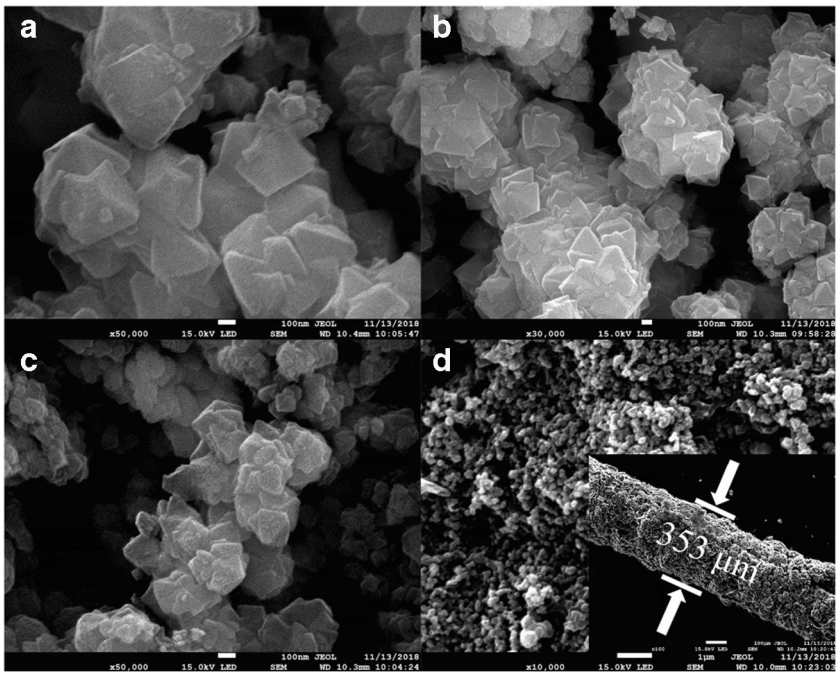

Fig. 3 SEM images of different coating: UiO-66-NH_2 (**a**), MWCNT/UiO-66-NH_2 (**b**), etched MWCNT/UiO-66-NH_2 (**c**) and PANI-etched MWCNT/UiO-66-NH_2 (**d**), (Inset: a larger version of the modified steel wire with 100 magnifications)

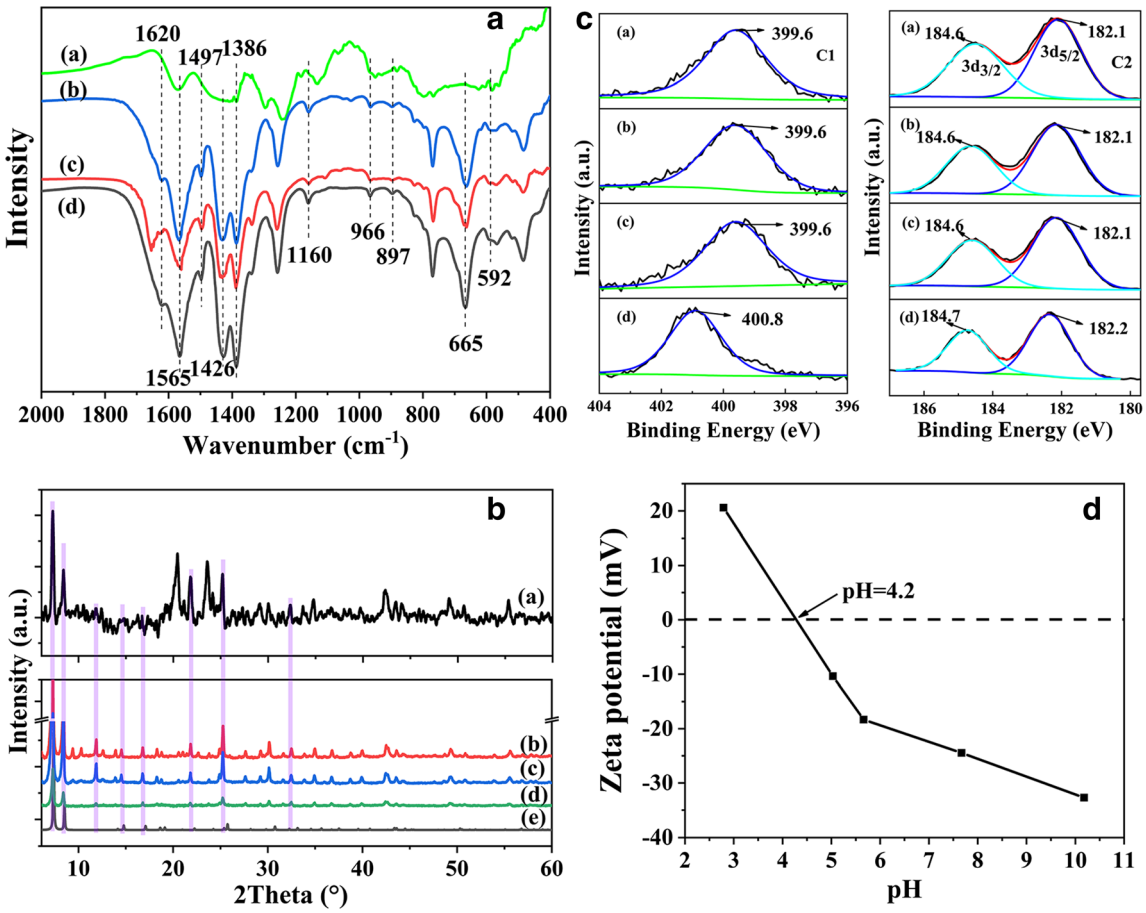

Fig. 4 FT-IR spectra (**a**) and XRD patterns (**b**) of different matrials: PANI-etched MWCNT/UiO-66-NH_2 (a), UiO-66-NH_2 (b), MWCNT/UiO-66-NH_2 (c), etched MWCNT/UiO-66-NH_2 (d) and simulated UiO-66-NH_2 (e); XPS: high revolution (**c**) of N 1 s spectra (C1) and Zr 3d spectra (C2) before (d) and after adsorbing pyrene (a), fluoranthene (b) and phenanthrene (c), respectively; A plot of the Zeta potential and pH of the composite coating (**d**)

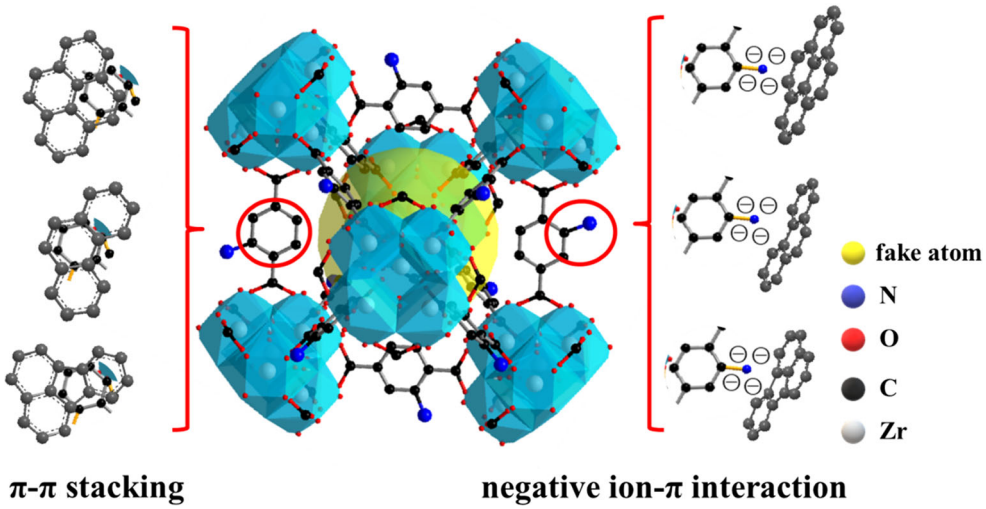

Fig. 5 Mechanism simulation for the adsorption of PAHs with composite coating materials

completion of the electropolymerization, the prepared stainless-steel wire was washed 3 times with ultrapure water, and dried for subsequent experiments. The preparation process is shown in Fig. 1. The optimization of preparing condition was in the supplementary material, Fig. S1.

SPME-HPLC procedure

10 mL of 10 ng mL^{-1} PAHs standard working solution (pH = 5.0) was added to a centrifuge tube with a rubber stopper inserted with a PANI-etched MWCNT/UiO-66-NH_2 coated fiber. The centrifuge tube was sealed with the above rubber stopper, and the vortex was shaken for 30 min for extraction. After the extraction was completed, the fiber was taken out and inserted into a small rubber stopper which was used for sealing a pipette tip containing 300 μL methanol, and the whole pipette tip was eddied for 10 min for elution.

When the SPME procedure was finished, the above methanol solution was analyzed by HPLC. Chromatographic conditions: mobile phase was methanol: water (9:1); detection wavelengths of phenanthrene, fluoranthene and pyrene were 250 nm, 236 nm and 239 nm, respectively; column temperature was 45 °C and flow rate was 1 mL min^{-1}. The SPME-HPLC procedure is shown in Fig. 2.

Results and discussion

Characterization of PANI-etched MWCNT/UiO-66-NH_2

Figure 3 shows the microscopic morphology of the different coatings. It can be seen that the pure UiO-66-NH_2 was composed of a plurality of octahedrons with a smooth surface and sharp edges (Fig. 3a). After doped with MWCNTs, these multiple octahedrons became significantly denser (Fig. 3b). The presence of MWCNTs was barely observed because they may be covered by UiO-66-NH_2 [18, 29]. After etched by acetic acid, the overall structure of the MWCNT/UiO-66-NH_2 composite material did not change significantly. The structure of multiple octahedrons was maintained, indicating that the overall structure of the crystal was not destroyed after etching. However, the surface of each crystal face become significantly rough and the edges were rounded (Fig. 3c). Figure 3d shows that the PANI

Table 1 Analytical performance of the established method for the determination of PAHs

Analytes	LRs [a]	Linearity equation	LODs	LOQs	RSD (%) ($n = 5$) (One fiber / Fiber to fiber)
Phenanthrene	0.05–20	Y = 0.16X + 0.05 [b] $R^2 = 0.9975$	0.01	0.03	1.4 / 6.3
Fluoranthene	0.05–20	Y = 0.09X + 0.09 $R^2 = 0.9940$	0.01	0.03	1.5 / 6.2
Pyrene	0.05–20	Y = 0.14X + 0.02 $R^2 = 0.9911$	0.01	0.03	1.4 / 6.5

[a] All concentration units in the table were "ng mL^{-1}"

[b] Y: peak area; X: concentration of analyte

Table 2 Comparison of SPME-HPLC methods with different sorbents for PAHs analytes

Sorbents	Detections	LRs (ng mL^{-1})	LODs (ng L^{-1})	RSD (%)	Reference
POSS-epoxy/TMOS+MTMOS [a]	GC-MS [c]	0.001–0.2	0.1–0.3	10–12	[36]
PAF-6 [b]	GC-MS	0.0016–4.0	0.8–4.2	7.1–9.6	[37]
PANI-etched MWCNT/UiO-66-NH_2	HPLC-DAD	0.05–20	10	6.2–6.5	This work

[a] Epoxy-modified polyhedral oligomeric silsesquioxane with tetramethylorthosilicate and ethyltrimethoxysilane

[b] Porous aromatic frameworks-6 synthesized by a one-step reaction of cyanuric chloride with piperazine

[c] Gas chromatography-mass spectrometry

doped etched MWCNT/UiO-66-NH_2 coating exhibited a porous network structure with a typical of polymers like PANI. Since the diameter of the steel wire was 250 μm, the thickness of the coating was about 51 μm (Inset of Fig. 3d).

Figure 4a shows the difference between the infrared spectra of diverse coatings. The absorption peaks at 1565 and 1386 cm^{-1} were due to the asymmetric and symmetric stretching of ν (O-C=O), respectively. The bands at 1620, 1497 and 1426 cm^{-1} were the typical vibration of ν (C=C) in a benzene ring. The peaks at 1000 cm^{-1} may be ascribed to the stretching vibrations of Zr-O in UiO-66-NH_2. The peak at 665 cm^{-1} can be ascribed to μ_3-O stretching in the cluster of $Zr_6O_4(OH)_4(-CO_2)_{12}$. And the bond at about 592 cm^{-1} can be assigned to the asymmetric stretching vibration of Zr-O_2. The presence of these absorption peaks indicated that the MWCNT/UiO-66-NH_2 complex had been successfully doped into the PANI coating.

XRD patterns of different coating materials were evaluated to observe any change in the crystal form by comparison with the simulated UiO-66-NH_2. In Fig. 4b, there are eight main characteristic peaks at 2θ = 7.3°, 8.4°, 12.0°, 14.6°, 16.8°, 21.8°, 25.2°, 32.4° which were assigned to the (111), (002), (022), (004), (400), (115), (442) and (137) planes of UiO-66-NH_2. The existence of these diffraction peaks indicated that the crystal structure of UiO-66-NH_2 had no significant change during the preparation of composite coating, which was consistent with the results of SEM.

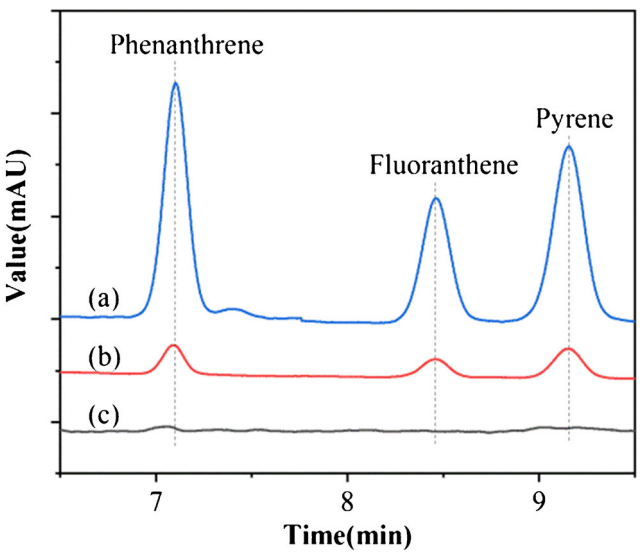

Fig. 6 Chromatograms of lake water spiked at 5 ng mL^{-1} PAHs after (**a**) and before (**b**) SPME; blank lake water after SPME (**c**)

Adsorption mechanisms

The interaction between PAHs and the composite was studied by FT-IR, XPS, and Zeta potential. In the infrared spectra (Fig. S3A), the absorption peak of C=C was obviously enhanced after the adsorption of PAHs, indicating there was π stacking between the composite and PAHs [30]. Additionally, the intensity of ν (Ar-N) grew markedly, which meant that the amino group on the benzene ring in UiO-66-NH_2 also interacted with the π bond of PAHs. XPS spectra show that the binding energy of N 1 s changed from 400.8 eV to 399.6 eV after adsorption (Fig. S3B, Fig. 4C1). The decrease in the electron binding energy of the inner layer indicated that the outer electron density of N increased due to the adsorption of PAHs. For Zr, the combined energy of the 3d orbit was only reduced by 0.1 eV, and there was almost no changed (Fig. 4C2). The results showed that the amino group on the composite adsorbed with PAHs, while Zr did not provide additional adsorption sites, which was consistent with the conclusion of infrared spectroscopy. Figure 4d shows the isoelectric point of the coating was about at pH = 4.2. The optimum extraction acidity was proved to be pH = 5.0 (Fig. S2C), which indicated that the surface of coating was negatively charged during extraction. Combined with the results of XPS spectrum, there may be an anion-π interaction between the negatively charged amino group on the composite and PAHs [31, 32]. However, as the pH continued to rise, the extraction effect began to decrease. It was probably because the excessive surface charge and hydrophilicity were not beneficial to the adsorption of PAHs.

In summary, the composite coating with abundant benzene ring can easily undergo π stacking with PAHs [33–35]. At the same time, there is anion-π interaction between the negatively charged composite and PAHs under the optimal pH condition. The mechanism simulation for the adsorption of PAHs with

Table 3 Recoveries for the determination of the PAHs in water samples ($n = 3$)

Analytes	Spiked [a]	Sha Lake			Yanxi Lake		
		Found	Recovery	RSD	Found	Recovery	RSD
Phenanthrene	0	2.2	–	–	1.2	–	–
	10	11.0	88.0%	10.2%	10.1	89.0%	7.1%
Fluoranthene	0	7.1	–	–	0.3	–	–
	10	15.8	87.0%	9.7%	9.3	90.0%	13.2%
Pyrene	0	0.6	–	–	0.9	–	–
	10	10.8	102.0%	11.5%	10.1	92.0%	8.4%

[a] All concentration units in the table were "ng mL^{-1}"

composite coating is shown in Fig. 5. The left and right side of the figure shows the π stacking and the negative ion-π interaction between them respectively. For convenience of expression, PANI, MWCNTs and all H atoms are omitted from the figure, and three PAHs are drawn in gray to distinguish C atoms in MOFs. The composite coating may be a promising absorbent for the similar analytes with large conjugation structure, and the amine or phenolic analytes with opposite charge.

Optimization of method

A SPME/HPLC method for the detection of PAHs was established after the extraction procedure based on the composite coating. The following parameters for the extraction of PAHs were optimized: (A) type of eluent; (B) NaCl concentration; (C) pH of the sample solution; (D) extraction time and (E) elution time. Respective text and Figures on optimizations were given in the Supplementary Material (Fig. S2). In short, the following experimental conditions were found to give best results: (A) type of eluent: MeOH; (B) optimal NaCl concentration: 0% (*w*/*v*); (C) best sample pH value: 5; (D) optimum extraction time: 30 min and (E) optimum elution time: 10 min.

Method evaluation

The analytical performance of the SPME/HPLC method for the detection of PAHs was evaluated under optimal conditions by extracting a standard dilution of a blank spiked lake water. Linear ranges (LRs), limits of detections (LODs, $S/N = 3$), limits of quantifications (LOQs, $S/N = 10$) and relative standard deviations (RSDs) are presented in Table 1. The LRs of phenanthrene, fluoranthene and pyrene were in the range of 0.05–20 ng mL^{-1}. The LODs were 0.01 ng mL^{-1}, and the LOQs were 0.03 ng mL^{-1}. The RSDs of one fiber and fiber to fiber ranged from 1.4% to 1.5% and 6.2% to 6.5%, respectively. The upper limit concentration of the linear range was low (20 ng mL^{-1}), which may limit the analytical application for the high concentration of PAHs. The established method had also been compared with some reported methods with the sorbent of POSS-epoxy/TMOS+MTMOS [36] and PAF-6 [37] (Table 2). These methods used mass spectrometry as detector, which sensitivity was higher than that of the ultraviolet detector. Although the LOD of the new method was not lower, its lower RSD indicated its good reproducibility. In addition, the cost of the new method was lower than the methods equipped with mass spectrometry.

Analysis of PAHs in water samples

The blank lake water spiked samples (5 ng mL^{-1}) before and after SPME were firstly analyzed by HPLC. The chromatograms are shown in Fig. 6, which proved that the three PAHs were well enriched by the PANI-etched MWCNT/UiO-66-NH_2 composite (curve a). Then, the developed method was applied to detect PAHs in real water samples from Sha Lake and Yanxi Lake. The qualitative of PAHs in water was determined by the retention time of the chromatogram, and their quantities was calculated from the calibration plot. As shown in Table 3, the three PAHs were detected in the two real water samples, ranging from 0.3 to 7.1 ng mL^{-1}. And the determined recoveries were in the range from 87.0% to 102.0%. These results indicated that the developed method exhibited satisfactory reliability and applicability for the determination of the PAHs in water source.

Conclusion

A novel PANI-doped MWCNT/UiO-66-NH_2 composite coating was prepared by electropolymerization, which was used for the preconcentration of PAHs by SPME. The adsorption mechanism was proved that the π stacking and negative ions-π interaction played dominate roles between the composite and PAHs. Coupled with HPLC, a sensitive and simple detection method for PAHs in water source was established, which had wide linear detection range, low LOD, satisfactory precision and accuracy. The analytical method was superior in lower cost and better reproducibility compared to other

methods with mass spectrometric detection. The work also provided an alternative strategy to prepare new composite material with superior properties.

Acknowledgements This research is supported by the National Nature Science Foundation of China (No. 61301048) and the Natural Science Fund for Creative Research Groups of Hubei Province of China (No. 2011CDA111)

References

1. Lupica-Spagnolo L, Ward DJ, Marie JJ, Lymperopoulou S, Bradshaw D (2018) Pollen-like ZIF-8 colloidosomes via emulsion templating and etching. Chem Commun 54(61):8506–8509. https://doi.org/10.1039/c8cc03511c
2. Kim H, Lah MS (2017) Templated and template-free fabrication strategies for zero-dimensional hollow MOF superstructures. Dalton Trans 46(19):6146–6158. https://doi.org/10.1039/c7dt00389g
3. Liu W, Huang J, Yang Q, Wang S, Sun X, Zhang W, Liu J, Huo F (2017) Multi-shelled hollow metal-organic frameworks. Angew Chem Int Ed 56(20):5512–5516. https://doi.org/10.1002/anie.201701604
4. Avci C, Arinez-Soriano J, Carne-Sanchez A, Guillerm V, Carbonell C, Imaz I, Maspoch D (2015) Post-synthetic anisotropic wet-chemical etching of colloidal sodalite ZIF crystals. Angew Chem Int Ed 54(48):14417–14421. https://doi.org/10.1002/anie.201507588
5. Shah M, McCarthy MC, Sachdeva S, Lee AK, Jeong H-K (2012) Current status of metal–organic framework membranes for gas separations: promises and challenges. Ind Eng Chem Res 51(5):2179–2199. https://doi.org/10.1021/ie202038m
6. Riccò R, Liang W, Li S, Gassensmith JJ, Caruso F, Doonan C, Falcaro P (2018) Metal-organic frameworks for cell and virus biology: a perspective. ACS Nano 12(1):13–23. https://doi.org/10.1021/acsnano.7b08056
7. Salunkhe RR, Kaneti YV, Yamauchi Y (2017) Metal-organic framework-derived Nanoporous metal oxides toward supercapacitor applications: progress and prospects. ACS Nano 11(6):5293–5308. https://doi.org/10.1021/acsnano.7b02796
8. Jia Y, Su H, Wang Z, Wong YE, Chen X, Wang M, Chan TD (2016) Metal-organic framework@microporous organic network as adsorbent for solid-phase microextraction. Anal Chem 88(19):9364–9367. https://doi.org/10.1021/acs.analchem.6b03156
9. Bradshaw D, El-Hankari S, Lupica-Spagnolo L (2014) Supramolecular templating of hierarchically porous metal–organic frameworks. Chem Soc Rev 43(16):5431–5443. https://doi.org/10.1039/C4CS00127C
10. Yue Y, Fulvio PF, Dai S (2015) Hierarchical metal-organic framework hybrids: perturbation-assisted nanofusion synthesis. Acc Chem Res 48(12):3044–3052. https://doi.org/10.1021/acs.accounts.5b00349
11. Singh V, Guo T, Xu H, Wu L, Gu J, Wu C, Gref R, Zhang J (2017) Moisture resistant and biofriendly CD-MOF nanoparticles obtained via cholesterol shielding. Chem Commun 53(66):9246–9249. https://doi.org/10.1039/c7cc03471g
12. Okpalugo TIT, Papakonstantinou P, Murphy H, McLaughlin J, Brown NMD (2005) High resolution XPS characterization of chemical functionalised MWCNTs and SWCNTs. Carbon 43(1):153–161. https://doi.org/10.1016/j.carbon.2004.08.033
13. Zhao Y, Chen H, Li J, Chen C (2015) Hierarchical MWCNTs/Fe_3O_4/PANI magnetic composite as adsorbent for methyl orange removal. J Colloid Interface Sci 450:189–195. https://doi.org/10.1016/j.jcis.2015.03.015
14. Chen J, Jia X, She Q, Wang C, Zhang Q, Zheng M, Dong Q (2010) The preparation of nano-sulfur/MWCNTs and its electrochemical performance. Electrochim Acta 55(27):8062–8066. https://doi.org/10.1016/j.electacta.2010.01.069
15. Aboutalebi SH, Chidembo AT, Salari M, Konstantinov K, Wexler D, Liu HK, Dou SX (2011) Comparison of GO, GO/MWCNTs composite and MWCNTs as potential electrode materials for supercapacitors. Energy Environ Sci 4(5):1855. https://doi.org/10.1039/c1ee01039e
16. Baughman RH, Zakhidov AA, De Heer WA (2002) Carbon nanotubes–the route toward applications. Science 297(5582):787–792. https://doi.org/10.1126/science.1060928
17. Coleman JN, Khan U, Blau WJ, Gun'ko YK (2006) Small but strong: a review of the mechanical properties of carbon nanotube–polymer composites. Carbon 44(9):1624–1652. https://doi.org/10.1016/j.carbon.2006.02.038
18. Qasem NAA, Qadir NU, Ben-Mansour R, Said SAM (2017) Synthesis, characterization, and CO_2 breakthrough adsorption of a novel MWCNT/MIL-101(Cr) composite. J CO2 Util 22:238–249. https://doi.org/10.1016/j.jcou.2017.10.015
19. Minjia H, Chao T, Qunfang Z, Guibin J (2004) Preparation of polyaniline coating on a stainless-steel wire using electroplating and its application to the determination of six aromatic amines using headspace solid-phase microextraction. J Chromatogr A 1048(2):257–262. https://doi.org/10.1016/j.chroma.2004.07.059
20. Li X, Zhong M, Chen J (2008) Electrodeposited polyaniline as a fiber coating for solid-phase microextraction of organochlorine pesticides from water. J Sep Sci 31(15):2839–2845. https://doi.org/10.1002/jssc.200800156
21. Bagheri H, Mir A, Babanezhad E (2005) An electropolymerized aniline-based fiber coating for solid phase microextraction of phenols from water. Anal Chim Acta 532(1):89–95. https://doi.org/10.1016/j.aca.2004.10.040
22. Lewis TW, Wallace GG, Smyth MR (1999) Electrofunctional polymers: their role in the development of new analytical systems. Analyst 124(3):213–219. https://doi.org/10.1039/A808015A
23. Lu C, Ben T, Xu S, Qiu S (2014) Electrochemical synthesis of a microporous conductive polymer based on a metal-organic framework thin film. Angew Chem Int Ed Engl 53(25):6454–6458. https://doi.org/10.1002/anie.201402950
24. Egardt J, Mork Larsen M, Lassen P, Dahllof I (2018) Release of PAHs and heavy metals in coastal environments linked to leisure boats. Mar Pollut Bull 127:664–671. https://doi.org/10.1016/j.marpolbul.2017.12.060
25. Stout SA, Payne JR, Emsbo-Mattingly SD, Baker G (2016) Weathering of field-collected floating and stranded Macondo oils during and shortly after the deepwater horizon oil spill. Mar Pollut Bull 105(1):7–22. https://doi.org/10.1016/j.marpolbul.2016.02.044
26. Farmer PB, Singh R, Kaur B, Sram RJ, Binkova B, Kalina I, Popov TA, Garte S, Taioli E, Gabelova A, Cebulska-Wasilewska A (2003) Molecular epidemiology studies of carcinogenic environmental pollutants. Mutat Res/Rev Mutat 544(2-3):397–402. https://doi.org/10.1016/j.mrrev.2003.09.002
27. Sram RJ, Svecova V, Rossnerova A (2016) Systematic review of the use of the lymphocyte cytokinesis-block micronucleus assay to measure DNA damage induced by exposure to polycyclic aromatic hydrocarbons. Mutat Res/Rev Mutat 770(Pt A):162–169. https://doi.org/10.1016/j.mrrev.2016.07.009
28. Zelinkova Z, Wenzl T (2015) The occurrence of 16 EPA PAHs in food - a review. Polycycl Aromat Compd 35(2-4):248–284. https://doi.org/10.1080/10406638.2014.918550

29. Chan Z, Miao F, Xiao Z, Juan H, Hongbing Z (2007) Effect of doping levels on the pore structure of carbon nanotube/silica xerogel composites. Mater Lett 61(3):644–647. https://doi.org/10.1016/j.matlet.2006.05.074
30. Wang J, Chen Z, Chen B (2014) Adsorption of polycyclic aromatic hydrocarbons by graphene and graphene oxide nanosheets. Environ Sci Technol 48(9):4817–4825. https://doi.org/10.1021/es405227u
31. Aragay G, Frontera A, Lloveras V, Vidal-Gancedo J, Ballester P (2013) Different nature of the interactions between anions and HAT(CN)6: from reversible anion-pi complexes to irreversible electron-transfer processes (HAT(CN)6 = 1,4,5,8,9,12-hexaazatriphenylene). J Am Chem Soc 135(7):2620–2627. https://doi.org/10.1021/ja309960m
32. Wang DX, Wang MX (2013) Anion-pi interactions: generality, binding strength, and structure. J Am Chem Soc 135(2):892–897. https://doi.org/10.1021/ja310834w
33. Bu Y, Feng J, Sun M, Zhou C, Luo C (2016) Facile and efficient poly(ethylene terephthalate) fibers-in-tube for online solid-phase microextraction towards polycyclic aromatic hydrocarbons. Anal Bioanal Chem 408(18):4871–4882. https://doi.org/10.1007/s00216-016-9567-z
34. Chen X, Chen B (2015) Macroscopic and spectroscopic investigations of the adsorption of nitroaromatic compounds on graphene oxide, reduced graphene oxide, and graphene nanosheets. Environ Sci Technol 49(10):6181–6189. https://doi.org/10.1021/es5054946
35. Hu X, Wang C, Li J, Luo R, Liu C, Sun X, Shen J, Han W, Wang L (2018) Metal-organic framework-derived hollow carbon Nanocubes for fast solid-phase microextraction of polycyclic aromatic hydrocarbons. ACS Appl Mater Interfaces 10(17):15051–15057. https://doi.org/10.1021/acsami.8b02281
36. Bagheri H, Soofi G, Javanmardi H, Karimi M (2018) A 3D nanoscale polyhedral oligomeric silsesquioxanes network for microextraction of polycyclic aromatic hydrocarbons. Microchim Acta 185(9):418. https://doi.org/10.1007/s00604-018-2950-z
37. Wang W, Li Z, Wang W, Zhang L, Zhang S, Wang C, Wang Z (2017) Microextraction of polycyclic aromatic hydrocarbons by using a stainless steel fiber coated with nanoparticles made from a porous aromatic framework. Microchim Acta 185(1):20. https://doi.org/10.1007/s00604-017-2577-5

Publisher's note Springer Nature remains neutral with regard to jurisdictional claims in published maps and institutional affiliations.